Precipitate Effects on the Mechanical Behavior of Aluminum Copper Alloys: Part II. Modeling

H. SEHITOGLU, T. FOGLESONG, and H.J. MAIER

This work focuses on a new hardening formulation accounting for precipitate-induced anisotropy in a binary aluminum-copper precipitation-hardened alloy. Different precipitates were developed upon aging at 190 °C and 260 °C, and corresponding work hardening characteristics were predicted for single and polycrystals. The use of single crystals facilitated the demonstration of the effect of precipitates on the flow anisotropy behavior. Pure aluminum was also studied to highlight the change in deformation mechanisms due to the introduction of precipitates in the matrix. The influence of precipitate-induced anisotropy on single-crystal flow behavior was clearly established, again relating to the precipitate character. Simulations are presented for several single-crystal orientations and polycrystals, and they display good agreement with experiments. The work demonstrates that precipitate-induced anisotropy can dominate over the crystal anisotropy effects in some cases.

I. INTRODUCTION

IN the first part of this series of articles, the deformation behavior of pure aluminum and an aluminum-4 wt. pct copper alloy as a function of crystal orientation and precipitate morphology was described. Since there are three different precipitates that can form, the yield strength and the work hardening coefficients change depending on the aging treatment. To develop a physically based model that has better capabilities than conventional plasticity models, it is necessary to understand how the microstructural picture changes with the deformation. Incorporating microstructural theory into the model provides a sound basis for predicting the mechanical response of a material.

Visco-plastic continuum models[1] for aluminum copper alloys have been investigated in a previous study with some success. These models do not explicitly incorporate texture effects and precipitate effects in polycrystalline and single crystalline materials.[2] The crystal plasticity models[3,4,5] have the versatility to account for the role of crystal orientation, or preferred texture, and can incorporate the dislocation evolution terms directly into the constitutive description. For example, as the mean free path of dislocation motion is governed by precipitate spacing, the crystal plasticity models take into account this lengthscale effect. Previous work on aluminum alloys has focused on single aging treatments. The current effort has focused on several aging treatments to create all possible precipitate types in aluminum-copper alloys.[6–9] The current motivation is to develop a comprehensive hardening law for different aging treatments.

This work attempts to develop a physically sound and comprehensive hardening law and uses a modified visco-plastic self-consistent (VPSC) polycrystal model that can be applied to precipitation-hardened alloys.[10] The materials to be studied in this work are pure aluminum and an aluminum-copper alloy in both single and polycrystalline forms. The pure aluminum represents a baseline for comparison. The choice of single-crystal specimens eliminates the complicating effects of grain boundaries and constraints imposed on one grain by neighboring grains. Single crystals have no contribution from grain boundary effects, and thus, work hardening only has components due to dislocation-dislocation interactions in the solutionized case; and in the aged samples, there are additional dislocation-precipitation interactions. In this manner, the various model parameters can be extracted from the single-crystal results. Studying the pure aluminum will highlight the dislocation-dislocation interactions in the matrix, as these will be the only obstacles to dislocation motion and will provide a comparison to the change in deformation mechanisms when precipitates are introduced into the matrix. The added complexity of precipitates will be incorporated into the model based on the mechanical response of the aluminum-copper alloy exposed to various aging treatments, as described in Part I. In these cases, the material's behavior becomes more complicated as there now exist not only dislocation-dislocation interactions in the matrix but also the additional dislocation-particle interactions due to the precipitates.

Microstructural lengthscales are not inherent in polycrystal models and must be added through a microscopic hardening law. Incorporating lengthscales into polycrystal models is an important modification, as the mechanical behavior of a material is dependent upon the slip length of dislocations. Any obstacle or interaction that impedes the motion of a dislocation or acts as a barrier to further dislocation motion changes the effective slip path of a dislocation. As a result, it is imperative that microstructural lengthscales be incorporated into material models to more accurately represent and predict the resulting mechanical behavior. Some common size effects and microstructural lengthscales important in determining mechanical behavior were reviewed in Reference 11 and described in Part I of this article.

Another issue to consider is the strength of the obstacle or barrier. For example, when precipitates are introduced into the matrix, their level of coherency with the matrix

H. SEHITOGLU, C.J. Ganthier Professor and Interim Head, is with the Department of Mechanical and Industrial Engineering, University of Illinois, Urbana, IL 61801. Contact e-mail: huseyin@uiuc.edu T. FOGLESONG formerly with the Department of Mechanical and Industrial Engineering, University of Illinois, Urbana, IL 61801, is Research Engineer, with Exxon Mobile Upstream Research Company, Houston, TX 77046. H.J. MAIER, Professor, is with the Department of Materials Science, University of Paderborn, D-33905 Paderborn, Gemany.

dictates how the dislocations will interact with the precipitate. If the lattice planes of the precipitate are coherent with those of the matrix, then a dislocation will be able to shear the precipitate. However, this does not occur until a certain critical stress is obtained at the interface due to the coherency strains and the elastic mismatch at the precipitate/matrix interface since the precipitate is constrained within the matrix. On the other hand, if the precipitates are incoherent with the matrix, *i.e.* they share no common lattice planes, they will present an impenetrable obstacle and the dislocation will no longer be able to continue on its path by shearing the precipitate. As a result, the dislocation will have to bypass the obstacle by bowing between the precipitates, avoiding the obstacle through cross-slip, or climbing onto an alternative slip system.

II. POLYCRYSTAL MODELING OF PRECIPITATION-HARDENED MATERIALS

In the present work, the VPSC polycrystal model of Lebensohn and Tomé[11–13] was modified to account for work hardening due to geometric dislocation storage and precipitate-induced anisotropy. Unlike the fully constrained models that require a very rigid interaction between grains, the interaction in the VPSC models can be altered by changing the linearization method that is used to relate the stress and strain state within the grain.[11–13] The relaxed constraints models are not the most appropriate for the materials and deformation conditions of the present investigation, as they best represent the elongated grains of heavily deformed materials. The VPSC model has accurately predicted the mechanical responses of both single-crystal and polycrystalline forms of different materials.[11–14] Its success lies on predicting texture during rolling of face-centered-cubic (FCC) aggregates and deformation of hexagonal close-packed materials. This model was modified to account for the Al-Cu alloy behavior at various stages of aging. The precipitate spacing and grain size were the microstructural length parameters used in the hardening formulation in addition to the weighting term for precipitate-induced anisotropy associated with the formation of semicoherent θ' precipitates.

A. *VPSC Model*

The VPSC model is based on the inclusion formalism of Eshelby and the crystallographic slip concepts of Taylor. Each grain is treated as an ellipsoidal visco-plastic inclusion embedded in, and interacting with, a homogeneous effective medium with the surrounding grains as the polycrystal aggregate. The polycrystalline aggregate is treated as many grains with random or crystallographic orientations of different volume fractions. The interaction between the grains can be treated as "hard" or "soft" depending on the coupling between the stress and associated strain rate deviations.

The first step in developing a material model is to define the constitutive equations that will relate the stress and strain rate. Due to the nature of polycrystal models, constitutive equations must be formulated for the stress and strain rate relationship at both the single-crystal and polycrystal level.

In general, a six-component vector can describe the stress and strain rate tensors as the tensors are second-order symmetric with six independent components. However, this model considers only plasticity so the stress and strain rate tensors can be described by five independent components. Because plastic deformation occurs by shear, it can be considered independent of the hydrostatic stress component; thus, only five independent components comprise each vector.

Plastic deformation takes place *via* shear on active slip systems. The resolved shear stress (τ_r^s) onto a slip system (s) is given by

$$\tau_r^s = m_i^s \sigma'_i \qquad [1]$$

where m_i^s is the vector form of the Schmid tensor and σ'_i is the deviatoric stress component. In a similar form, the plastic strain rate can be related to the shear strain rate on a slip system as follows:

$$\dot{\varepsilon}_i^{in} = m_i^s \dot{\gamma}^s \qquad [2]$$

where $\dot{\varepsilon}_i^{in}$ is the plastic strain rate and $\dot{\gamma}^s$ is the shear rate in a given system.

The shear rate generated on a given slip system can be expressed by a nonlinear rate-sensitive formulation:

$$\dot{\gamma}^s = \dot{\gamma}^o \left(\frac{\tau_r^s}{\tau_c^s} \right)^n \qquad [3]$$

in which n is the inverse of the rate-sensitivity coefficient (usually denoted m), $\dot{\gamma}^o$ is a reference shear rate, and τ_c^s is a threshold stress corresponding to the reference shear rate. The threshold stress can be considered as the critical resolved shear stress CRSS. Substituting gives

$$\dot{\gamma}^s = \dot{\gamma}^o \left(\frac{m_i^s \sigma'_i}{\tau_c^s} \right)^n \qquad [4]$$

The plastic strain rate, given in Eq. [2], can now be rewritten by substituting Eq. [4] into Eq. [2], resulting in the following expression:

$$\dot{\varepsilon}_i^{in} = \dot{\gamma}^o \sum_{s=1}^{S} m_i^s \left(\frac{m_j^s \sigma'_j}{\tau_c^s} \right)^n \quad \text{where } i = 1 \text{ to } 5 \qquad [5]$$

This formulation gives a constitutive equation for each grain in the polycrystal and is summed over all slip systems in the grain ($S = 12$ for a fcc crystal). Equation [5] is a system of five nonlinear equations that contains ten unknowns in the form of five strain rate components and five deviatoric stress components. Consequently, another set of five equations is required to solve for all of the unknowns. These equations are obtained by relating the strain rate and stress in each grain with the average strain rate and the average stress in the polycrystal *via* an interaction equation. This requires that a constitutive equation must first be formulated at the polycrystal level and then coupled with the constitutive law at the grain level, as established earlier. The two systems of equations must then be solved simultaneously using the self-consistent formulation that will be described later.

The development of the polycrystal constitutive law begins by first rewriting the grain level constitutive law, Eq. [5], as shown subsequently.

$$\dot{\varepsilon}_i^{in} = \left\{ \dot{\gamma}^o \sum_{s=1}^{s} \frac{m_i^s m_j^s}{\tau_c^s} \left(\frac{m_k^s \sigma'_k}{\tau_c^s} \right)^{n-1} \right\} \sigma'_j \qquad [6]$$

Equation [6] can now be written in a pseudo-linear form by replacing the expression in brackets with the secant visco-plastic compliance moduli ($M_{ij}^{c(\sec)}$) of the grain.

$$\dot{\varepsilon}_i^{in} = M_{ij}^{c(\sec)}(\sigma')\sigma'_j \quad [7]$$

$M^{c(\sec)}$ depends upon the deviatoric stress and the superscript c denotes the crystal. Similarly, Eq. [7] can be linearized using the tangent visco-plastic compliance moduli of the grain.

$$\dot{\varepsilon}_i^{in} = M_{ij}^{c(tg)}(\overline{\sigma'})\sigma'_j + \dot{\varepsilon}_o^i \quad [8]$$

The grain's secant and tangent moduli are related by the simple proportionality shown in Eq. [9]:

$$M_{ij}^{c(tg)} = nM_{ij}^{c(\sec)} \quad [9]$$

The same relationship holds for the moduli at the aggregate level. The polycrystal constitutive law can now be formulated by assuming that the overall polycrystal response can be described by constitutive equations similar to those established for the grain level behavior. Following this assumption, we can write the secant relationship as

$$\dot{E}_i^{in} = M_{ij}^{(\sec)}(\overline{\Sigma'})\overline{\Sigma}'_j \quad [10]$$

where $\dot{E}_i^{in}$ and $\overline{\Sigma}'_j$ are the polycrystal strain rate and deviatoric stress, respectively, and the $M_{ij}^{(\sec)}$ values are the polycrystal secant moduli. The constitutive relationship, using the tangent moduli, can be written in a similar manner as Eq. [10].

$$\dot{E}_i^{in} = M_{ij}^{(tg)}(\overline{\Sigma}')\overline{\Sigma}'_j + \dot{E}_i^0 \quad [11]$$

At this point, two constitutive laws have been generated, one at the grain level and the second to describe the polycrystal response. However, the two laws are currently independent of one another, and the system of ten unknowns still cannot be solved. Consequently, a relationship is required that will couple the two constitutive laws. Section B details the derivation of an interaction equation, using Eshelby's equivalent inclusion method,[15,16] which relates the constitutive laws and provides a means for simultaneously solving the two systems of equations.

B. *Strain-Hardening Formulation*

One of the goals of this modeling work was to determine a hardening law that could incorporate the different deformation mechanisms observed in the pure aluminum and aluminum-copper alloy materials. To model the stress-strain behavior of the Al-Cu alloy over a range of aging treatments, it was necessary to work with a strain hardening formulation that could account for the changing effectiveness of the different phases of precipitates as barriers to dislocation motion. Microstructural lengthscales, such as grain boundaries and precipitate spacing, are not intrinsically described by polycrystal models but instead need to be introduced artificially through hardening laws that are physically based on dislocation theory. For these reasons, the hybrid model of Estrin and Mecking[17,18] was chosen as the foundation for the strain hardening formulation used in this work.

The hybrid model is based on the earlier phenomenological model of Mecking and Kocks,[19] who proposed a structure evolution equation for the total dislocation density. The main assumption of this model was that the dislocation structure can be represented by a single structure parameter, the dislocation density, which describes the average dislocation distribution based on athermal storage and dynamic recovery. Estrin and Mecking added a geometrical storage contribution to the structure evolution equation to represent the effect of obstacles on the dislocation slip path. This hybrid model, so termed for the combination of statistical and geometric storage terms, is applicable to materials when the slip path length of dislocations is determined by both dislocation-dislocation interactions and by dislocation-barrier interactions. The model has been used successfully in past work.[20] The Mecking–Kocks model is applicable to situations in which dislocation storage is due to not only dislocation-dislocation interactions but also to dislocations that are impeded by precipitates, grain boundaries, *etc.* This model will be adapted to incorporate the effect of precipitate spacing on the hardening behavior of the material. The resulting evolution equation has the form

$$\dot{\rho} = \sum_i \left\{ \frac{K_0}{db} + k_1\sqrt{\rho} - k_2\rho \right\} |\dot{\gamma}_i| \quad [12]$$

where d is obstacle spacing, $\mathbf{b}$ is the magnitude of the Burgers vector, K_o is an effective strength parameter, k_1 and k_2 are constants, and $\dot{\gamma}_i$ is the shear rate on slip system i. The first two terms represent dislocation storage. The third term represents dislocation annihilation by dynamic recovery. The first storage term results from the accumulation and reduction in the slip length of dislocations due to geometric sources, such as precipitates and grain boundaries. The second term results from the athermal or statistical storage of dislocations resulting from the interaction of mobile dislocations with forest dislocations and is proportional to $\rho^{1/2}$.[17] The d^{-1} dependence of the geometric storage term also corresponds with the treatment of Estrin and Mecking.[17]

The flow stress at a given temperature and strain rate can be expressed by the Bailey–Hirsch relationship:

$$\tau - \tau_0 = \alpha\mu\,\mathbf{b}\sqrt{\rho} \quad [13]$$

where τ_0 is the initial yield stress, α is a constant on the order of unity, and μ is the shear modulus. Combining Eqs. [12] and [13] and differentiating with respect to time results in the following expression for the flow stress, where the hardening expression is multiplied by the sum of the operative shear strain rates in a given grain. This results in an isotropic hardening law for which the flow stress on each operative slip system is updated by an equivalent hardening increment.

$$\dot{\tau} = \left[\frac{K_o\alpha^2\mu^2\mathbf{b}}{2(\tau - \tau_o)d} + \left(k_1\frac{\alpha\mu\mathbf{b}}{2} + k_2\frac{\tau - \tau_o}{2} \right) \right] \sum_i |\dot{\gamma}_i| \quad [14]$$

The constants k_1 and k_2 can be defined as

$$k_1 = \frac{2\theta_o}{\alpha\mu\mathbf{b}}$$

$$k_2 = \frac{2\theta_o}{\tau_s - \tau_o}$$

where θ_o is the initial rate of hardening and τ_s is the saturation stress when geometric effects are not considered. The saturation stress is a function of temperature and strain rate. However, for the room-temperature conditions modeled in this work, the materials were rate insensitive so the saturation stress will be considered constant for a given material condition. Inserting the expressions for the constants given previously into and rearranging Eq. [14] results in the general formulation to describe the single-crystal strain hardening.

$$\dot{\tau} = \left[\frac{\alpha^2\mu^2 b}{2(\tau - \tau_o)}\left(\frac{K_{01}}{d_1} + \frac{K_{02}}{d_2}\right) + \theta_o\left(\frac{\tau_s - \tau}{\tau_s - \tau_o}\right)\right]\sum_i |\dot{\gamma}_i| \quad [15]$$

The first expression has been expanded to include multiple contributions from geometric obstacles, such as precipitates and grain boundaries. The precipitate spacing is defined by d_1 and the grain size is given by d_2. Their relative strengths are represented by K_{01} and K_{02}. The second term is the well-known Voce term.[21] If more than one type of precipitate is present in the matrix, such as θ' and θ, the first term can be expanded further to include a similar third component that includes the precipitate spacing of the second precipitate. To portray the physical picture more accurately, it would also be feasible to include the relative volume fractions of the two precipitates. However, accurately quantifying these volume fractions experimentally could be quite difficult, and as a first approximation, it would be reasonable to replace the volume fractions by weighting the contributions of the two precipitate hardening components relative to one another. This procedure was not used in this research because the transmission electron microscopy (TEM) images did not show a significant amount of secondary precipitate that would contribute to the hardening.

An important phenomenon observed in Al-Cu alloys aged to include θ' precipitates is precipitate-induced anisotropy. The addition of preferentially oriented precipitates imparts an anisotropic effect on the flow behavior that works in an opposite manner to the flow anisotropy dependent upon crystallographic orientation. As a result, normally soft orientations are hardened considerably more by precipitates than the hard orientations in both single crystals and textured polycrystals. The hardening formulation in combination with the VPSC polycrystal model will not be able to predict this precipitate-induced anisotropy, because the hardening contribution from precipitates is currently described independently of crystallographic orientation. A modification to the above strain hardening formulation is proposed that incorporates a weighting function that is dependent on the orientation of the grain, the orientation of the precipitates, and the precipitate morphology. The modified equation is shown as

$$\dot{\tau} = \left[\frac{\alpha^2\mu^2\mathbf{b}}{2(\tau - \tau_o)}\left(W\frac{K_{01}}{d_1} + \frac{K_{02}}{d_2}\right) + \theta_o\left(\frac{\tau_s - \tau}{\tau_s - \tau_o}\right)\right]\sum_i |\dot{\gamma}_i| \quad [16]$$

where W is the weighting function. Because the precipitates create the added anisotropy, only the precipitate hardening contribution is weighted.

The next step is to determine the weighting function that will be used in the hardening formulation. Two functions were chosen that arise from the elastic inclusion[7] and plastic inclusion[6] models. The forms of their hardening laws are shown as

$$\sigma_x = M\tau_m(1 - f) + f\bar{\sigma}_{ppt}\bar{N} \quad \text{plastic inclusion model}$$
$$\sigma_x = M\tau_m(1 - f) + 2\mu f\overline{\|\gamma\|}\varepsilon^p \quad \text{elastic inclusion model} \quad [17]$$

The terms $\bar{N}$ and $\overline{\|\gamma\|}$ in the two models describe anisotropy introduced by the precipitates. The $\bar{\sigma}_{ppt}$ is the effective flow strength of the precipitate, M (a scalar) is the Taylor factor, f is the volume fraction of precipitates, τ_m is the critical shear stress required for slip in the matrix, and ε^p is the plastic strain discontinuity at the particle/matrix interface that is associated with an elastic inclusion. Both models consider the effect of the same externally applied strain on the resulting strain state of the inclusion. However, the two models differ in their calculation of the resulting inclusion strain state because they assume different deformation modes of the inclusion. The plastic inclusion model assumes that the precipitates both deform and rotate to accommodate some of the shear strains. The elastic inclusion model uses a different approach by treating the precipitates as elastic inclusions that generate a long-range back stress within the matrix. Explicit forms for these two functions for plate-shaped precipitates were determined by Lyttle and Wert[22] for an axisymmetric test, where θ is the angle between the stress axis and the normal to the precipitate plane.

$$N = \frac{1}{2}\left(\frac{5 + 3\cos 4\theta}{2}\right)^{1/2}$$
$$\|\gamma\| = \frac{15 - 8\cos 2\theta + 9\cos 4\theta}{32} \quad [18]$$

The preceding expressions are for a single variant of the precipitate and must be evaluated for all three precipitate variants in a grain. The term describing the anisotropy in a grain, due to a set of inclusions on crystallographically equivalent habit planes, can be defined as a weighted average of the individual variant contributions:

$$\bar{N} = \Sigma f_i N_i$$
$$\overline{\|\gamma\|} = \Sigma f_i \|\gamma\|_i \quad [19]$$

where f_i is the volume fraction of total precipitates on a given variant. This formulation is most useful for stress-aged materials in which the precipitates exhibit preferential nucleation on one or two of the three habit planes. No loads were applied to the materials during aging in this work and the volume fractions of precipitates on the three habit planes were considered equal. The weighting functions will thus simply be expressed as

$$\bar{N} = 1/3\,(N_1 + N_2 + N_3)$$
$$\overline{\|\gamma\|} = 1/3\left(\|\gamma\|_1 + \|\gamma\|_2 + \|\gamma\|_3\right) \quad [20]$$

The individual weighting factors, $\|\gamma\|_i$'s, are obtained by substituting the angle between the stress axis and normal to the precipitate habit plane for variant i in Eq. [18]. Then, Eq. [20] is used to obtain the weighting function $\overline{\|\gamma\|}$ by considering all three variants. The weighting factor, *W,* is the same as $\overline{\|\gamma\|}$ if elastic anisotropy is used, which is the case in this article. Physically, the elastic inclusion theory better represents the precipitate behavior in the strain regimes of this work. No evidence was found to support the plastic inclusion theory, such as deformation or rotation of precipitates in accommodating plastic deformation, implying that the precipitates acted as elastic inclusions. However, both anisotropy theories will be used as the weighting function in the strain hardening formulation to determine which best represents the experimental results. These weighting functions are illustrated in Table I as a function of orientation and for the polycrystalline case. Similar trends were noted using both factors, preferentially enhancing the strength of soft orientations relative to hard orientations, as will be shown upon comparison of prediction of deformation in the [117] and [111] orientations.

C. *VPSC Polycrystal Model Simulations*

The parameters for the hardening expressions were determined from the [111] single-crystal experimental results for each aging condition and material. This orientation is the most appropriate for comparison, as it deforms on multiple slip systems similar to the polycrystal samples.[14] These parameters remained unchanged for the predictions of other single-crystal orientations and polycrystal experiments for a given heat treatment.

Texture measurements were performed on the polycrystalline samples that displayed a random texture after recrystallization. Therefore, the polycrystalline grain input file was comprised of 1000 randomly oriented and equiaxed grains. These results were verified by processing the initial texture measurements into a discrete grain file that was used as the input to the VPSC model. The results were very similar to those of the randomly generated grain input file. Orienting the grains in the same direction simulated the single crystals. We note that the reorientation of the grains (due to slip) is also accounted for in the simulations.

D. *Model Constants and Work Hardening Parameters*

For the pure aluminum experiments, the strain hardening results purely from dislocation-dislocation interactions, as evidenced by cell formation in the TEM images in Part I of this series of articles. The strengthening due to dislocation interactions follows the dislocation storage of the statistical term in the flow equations. The average grain size of the aluminum was 95 μm. However, the grain boundary term was not included in the simulations, as the flow stress has been determined to be primarily dependent upon the cell size,[23,24] which is included in the second term of the hardening law. The hardening parameters were determined from the [111] stress-strain curve and then held constant during the simulations. The values of τ_o, τ_s, and θ_o were determined as 3.5, 27, and 35 MPa, respectively. The magnitude of the Burger's vector, **b**, is 0.286 nm, and the constant α was set to 1/3.[17]

For the aluminum-copper simulations, the initial hardening rate of the matrix was higher than the value for pure aluminum. The TEM images from the samples depicted dislocation storage mainly due to the precipitates, and the precipitates are expected to control the work hardening of the material. The value θ_o was assumed to remain constant throughout the heat treatments as 150 MPa. The physical properties of the matrix change with aging treatment as the precipitates develop and coarsen, depleting the copper in solution. This change was reflected through modifying the τ_s term, as necessary, for different aging conditions. The average grain size for the Al-Cu samples was 70 μm and the average precipitate spacings ranged from 92 nm for the material aged 10 hours at 190 °C to 320 nm for the material aged 24 hours at 260 °C. The precipitate component of the hardening formulation, K_{01}/d_1, was changed with heat treatment. The variation of this ratio for the two aging treatments as a function of time is shown in Figure 1. Note that K_{01}/d_1 is not zero for the no-aging case, reflecting the presence of obstacles to dislocation motion. In the case of pure aluminum, the K_{01}/d_1 is set to zero. For both temperatures, the hardening value increases to a peak level with increasing aging time and then saturates to a constant value. If the aging time were increased to many hours, up to 1000 hours at 260 °C, for example, it would be expected that this ratio would decrease, reflecting the extreme overaging conditions.

Table I. Evaluation of the Two Weighting Functions for Different Single-Crystal Orientations and a Randomly Oriented Polycrystal

Compression Axis Direction	W (Plastic Inclusion)	W (Elastic Inclusion)
[111]	0.5774	0.333
[123]	0.6900	0.4583
[117]	0.9611	0.7762
[112]	0.7016	0.4583
[100]	1.00	0.833
Polycrystal	0.7711	0.4688

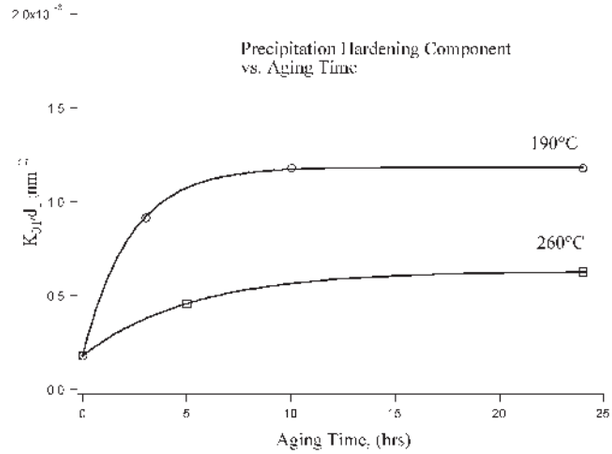

Fig. 1—Variation of precipitate hardening contribution with respect to aging time and temperature.

We use the precipitate spacing as a guide in establishing the trends in the constants, but the exact values of the parameters (such as K_{01}/d_1) come from the experimental stress-strain curves for the [111] orientation.

The precipitate hardening ratio for the material aged at 190 °C was consistently greater than the material aged at 260 °C. The relationship follows a similar trend to that observed when plotting aging curves of hardness *vs* time for different aging temperatures. The aging curves established by Hardy[25] showed that as the aging temperature increased from 190 °C to 240 °C, the peak hardness decreased. The lower temperature aging provided a more even distribution of precipitates, effectively trapping and opposing dislocation motion, resulting in higher work hardening rates.

E. *Simulations for Aluminum and Aged Aluminum-Copper Alloy*

The results of the simulations for pure aluminum are given in Figure 2. An accurate simulation was obtained for the [111] orientation and the correct trends were obtained for the polycrystal and the [117] experimental data. The simulations exhibited increased hardening over the experimental stress-strain curves. The experiments were repeated several times to ensure consistency of results. Because the [117] orientation lays on the boundary of the stereographic triangle, it has two favorably oriented systems from the onset of plastic deformation. The polycrystal model required more than two slip systems to be operative in order to maintain compatibility and equilibrium so it would be expected to generally overpredict stresses at those orientations that do not deform *via* polyslip.

Comparisons between the experiments and aluminum-copper alloy simulations for different aging treatments are displayed in Figures 3 through 8. The hardening parameters were determined from the [111] experimental results and then held constant for the remainder of the simulations for that aging treatment. The only additional parameter used for the polycrystal simulations was to include a contribution from the grain boundaries that was considered the same for

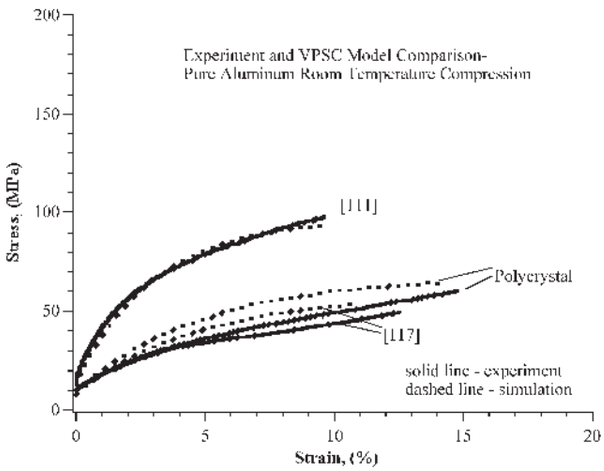

Fig. 2—Comparison of room-temperature compression experiments and simulations for the pure aluminum single and polycrystals.

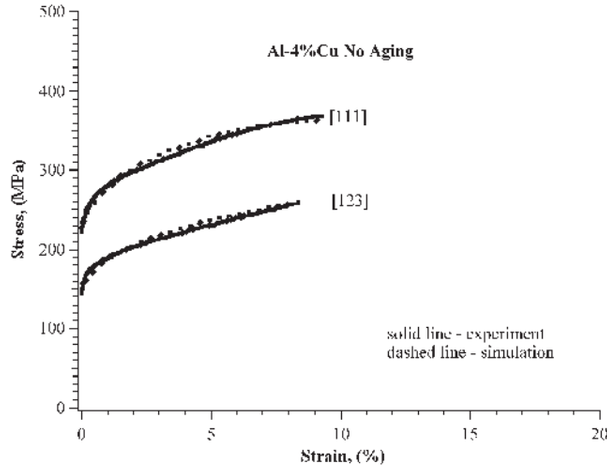

Fig. 3—Comparison of room-temperature compression experiments and simulations for the Al-4 wt pct Cu single crystals with no artifical aging.

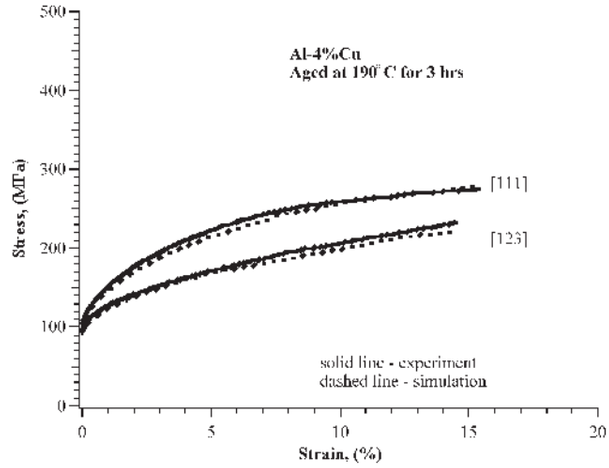

Fig. 4—Comparison of room-temperature compression experiments and simulations for the Al-4 wt pct Cu single crystals aged at 190 °C for 3 h.

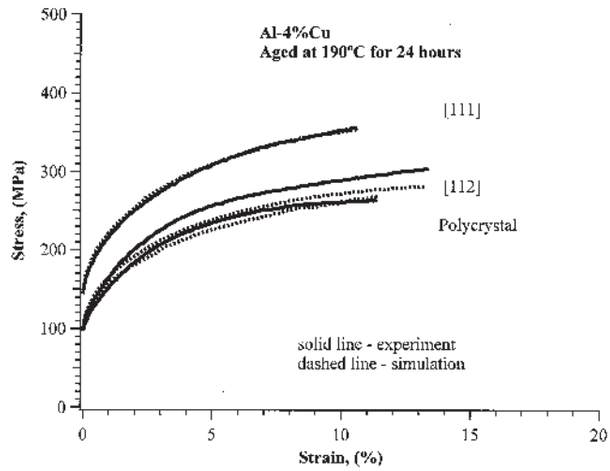

Fig. 5—Comparison of room-temperature compression experiments and simulations for the Al-4 wt pct Cu single and polycrystals aged at 190 °C for 24 h.

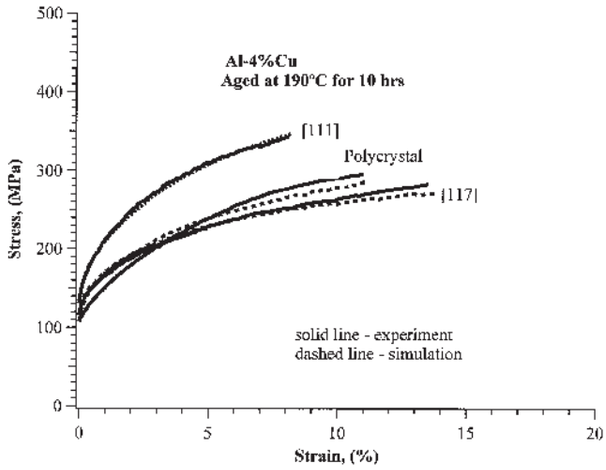

Fig. 6—Comparison of room-temperature compression experiments and simulations for the Al-4 wt pct Cu single and polycrystals aged at 190 °C for 10 h.

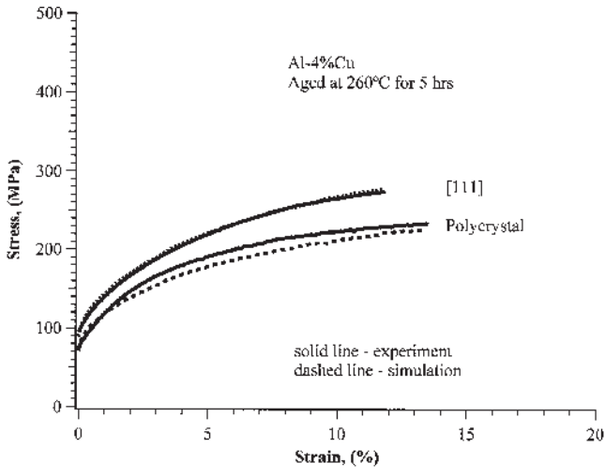

Fig. 7—Comparison of room-temperature compression experiments and simulations for the Al-4 wt pct Cu single and polycrystals aged at 260 °C for 5 h.

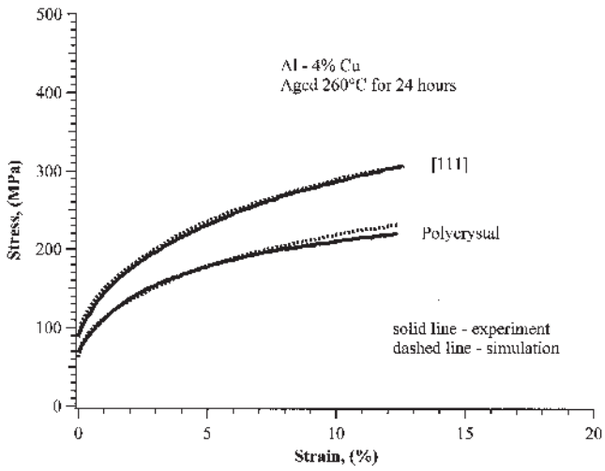

Fig. 8—Comparison of room-temperature compression experiments and simulations for the Al-4 wt pct Cu single and polycrystals aged at 260 °C for 24 h.

all aging treatments. A summary of all the constants used in this work is given in Table II. In Table II, SC denotes single crystal and PC denotes polycrystal.

In Figure 3, the results are displayed for the aluminum-copper material with no artificial aging. The material with no artificial aging contains Guinier–Preston zones that do not contribute to precipitate-induced anisotropy, and crystallographic effects dominate in this case. The work hardening parameters τ_o, τ_s, and θ_o were taken as 54, 95, and 150 MPa, respectively. The value of θ_o was maintained the same during the remainder of the simulations. The results for the alloy aged at 190 °C for 3 hours are shown in Figure 4, and the microstructure indicated the presence of nonequilibrium precipitates. The results point to a decrease in crystallographic orientation dependence for this case and the ability to accurately simulate the [123] orientation using the parameters from [111]. The work hardening parameters τ_o and τ_s were taken as 31.5 and 75 MPa, respectively. The K_{01}/d_1 is given in Figure 1.

The results for the aluminum-copper alloy aged at 190 °C for 10 and 24 hours are given in Figures 5 and 6, respectively. In these cases, the precipitates became well developed and precipitate-induced anisotropy narrowed the difference between [111] and other orientations. The TEM images, recorded after deformation, showed no precipitates that rotated, plastically deformed, or sheared during compression. It was concluded from these observations that the precipitates contributing to the anisotropy behaved as non-shearable, elastic inclusions. For higher strain levels, the weighting factor derived from the plastic inclusion theory would be more appropriate. The [111] and the polycrystalline simulations were in good agreement with the experiments. The presence of the precipitates in the matrix also forced the single-crystal orientations that normally slip on only one or two systems to now deform on multiple slip systems. The simulations for the [112] orientation fall slightly short of the experimental stress levels because the weighting function alone was simply not adequate to describe the dramatic increase in the work hardening rates for the [112] case. The work hardening parameters τ_o and τ_s were taken as 38 and 95 MPa, respectively, for the 190 °C, 10-hour treatment and 39 and 85 MPa, respectively, for the 24-hour treatment. The K_{01}/d_1 levels are given in Figure 1. For the polycrystalline simulations, the K_{02}/d_2 value was 3.06×10^{-4} (Table II).

Simulations for the aging treatment at 260 °C for 5 hours are shown in Figure 7. Again, the work hardening formulation accurately simulated the [111] orientation and provided accurate predictions of the polycrystal experiments. The work hardening parameters τ_o and τ_s were taken as 26.2 and 78 MPa, respectively, and the K_{01}/d_1 value is given in Figure 1.

The simulations for the 260 °C, 24-hour aging case are shown in Figure 8, displaying good agreement with the experiments. The work hardening parameters τ_o and τ_s were 25.5 and 85 MPa, respectively. In all of the simulations, the weighting factor from elastic inclusion theory was used; however, when the plastic inclusion theory was used in the hardening formulation, the results produced were very similar, with the exception of the [117] orientation, in which the plastic inclusion simulation stresses fell even lower than those predicted by the elastic inclusion factor. Experimentally, both assumptions can be considered valid depending on the strain regime of the experiment, with elastic inclusion treatment providing a more accurate physical representation for the compression experiments in this study. Both elastic

Table II. Hardening Parameters for Pure Aluminum and Al-4 wt pct Cu with Different Heat Treatments (SC = Single Crystal, PC = Polycrystal)

Sample Type	Heat Treatment	τ_o (MPa)	τ_s (MPa)	θ_o (MPa)	$\frac{K_{01}}{d_1}$ (nm^{-1})	$\frac{K_{02}}{d_2}$ (nm^{-1})
SC	pure aluminum	3.5	27	35	—	—
PC	pure aluminum	3.5	27	35	—	—
SC	no aging	54	95	150	1.84×10^{-4}	—
PC	no aging	54	95	150	1.84×10^{-4}	3.06E-4
SC	190 °C, 3 h	31.5	75	150	9.18×10^{-4}	—
PC	190 °C, 3 h	31.5	75	150	9.18×10^{-4}	3.06E-4
SC	190 °C, 10 h	38	95	150	1.18×10^{-3}	—
PC	190 °C, 10 h	38	95	150	1.18×10^{-3}	3.06E-4
SC	190 °C, 24 h	39	85	150	1.18×10^{-3}	—
PC	190 °C, 24 h	39	85	150	1.18×10^{-3}	3.06E-4
SC	260 °C, 5 h	26.2	78	150	4.59×10^{-4}	—
PC	260 °C, 5 h	26.2	78	150	4.59×10^{-4}	3.06E-4
SC	260 °C, 24 h	25.5	85	150	6.29×10^{-4}	—
PC	260 °C, 24 h	25.5	85	150	6.29×10^{-4}	3.06E-4

and plastic inclusion models deliver weighting factors that show similar trends in terms of enhancing the strength of crystallographically soft orientations relative to hard orientations, but the magnitude of the corrections is different.

III. SUMMARY OF FINDINGS

The work demonstrated that the nature of the precipitates in aluminum copper alloys have a profound effect on the work hardening behavior. The geometrically necessary dislocation evolution term incorporating K_{01}/d_1 is strongly dependent on both the aging temperature and the aging time. With the appropriate choice of K_{01}/d_1, all the precipitate structures encountered in Al-Cu alloys can be described. The precipitation-induced anisotropy term, *W,* modifies the geometrically necessary dislocation evolution term and considerably modifies the crystal anisotropy.

The preceding formulation is incorporated into a VPSC polycrystal code. The parameters for the strain hardening formulation were determined from the [111] single-crystal experiments and held constant for the polycrystal and other single-crystal simulations. The use of the constants obtained from single-crystal experiments with multiple slip orientations is favored over establishing the constants from polycrystalline data. As such, it was remarkable that the constants described the polycrystalline behavior very accurately for most cases.

The results point out that the materials artificially aged to produce precipitates exhibit less anisotropy compared to no aging cases. Therefore, the precipitation-hardened aluminum alloy behavior cannot be described simply by a Taylor-type analysis nor can texture strengthening be used as an effective means of directionally hardening the material.

ACKNOWLEDGMENTS

The work is partially sponsored by the Ford Motor Company (Dearborn, MI), the Fracture Control Program, University of Illinois, and the National Science Foundation (Grant No. DMR-0313489). The Frederick Seitz Materials Research Laboratory Facilities, supported by US Dept. of Energy Grant DEF 02-91ER45439, were utilized in 'texture' portion of the work. The authors acknowledge discussions with C. Tome on the VPSC code modification.

REFERENCES

1. H. Sehitoglu, X. Qing, T.J. Smith, H.J. Maier, and J.A. Allison: *Metall. Mater. Trans. A,* 2000, vol. 31A, pp. 139-51.
2. T.J. Foglesong, H. Sehitoglu, and H.J. Maier: *J. Phys. IV,* 2003, vol. 105, pp. 239-46.
3. G.I. Taylor: *J. Inst. Met.,* 1938, vol. 62, pp. 307-24.
4. J.F.W. Bishop, and R. Hill: *Phil. Mag.,* 1951, vol. 42, pp. 414-27.
5. B. Budiansky, and T.T. Wu: *Proc. 4th U.S. Nat. Congr. on Applied Mechanics,* 1962, vol. 2, pp. 1175-85.
6. W.F. Hosford, and R.H. Zeisloft: *Metall. Trans.,* 1972, vol. 3, pp. 113-21.
7. P. Bate, W.T. Roberts, and D.V. Wilson: *Acta Metall.,* 1981, vol. 29 (11), pp. 1797-1814.
8. F. Barlat, and J. Liu: *Mater. Sci. Eng. A: Struct. Mater. Prop. Microstr. Processing,* 1998, vol. A257, pp. 47-61.
9. P. Sainfort, X. Dufaure de Citres, Y. Brechet, P. Lipinski, and M. Berveiller: *Proc. 3rd Int. Conf. on Aluminium Alloys,* Trondheim, Norway, 1992, pp. 483-88.
10. E. Arzt: *Acta Mater.,* 1998, vol. 46 (16), pp. 5611-26.
11. R.A. Lebensohn and C.N. Tomé: *Acta Metall. Mater.,* 1993, vol. 41 (9), pp. 2611-24.
12. C.N. Tomé: *Modelling Simulation in Mater. Sci. Eng.,* 1999, vol. 7, pp. 723-38.
13. R.A. Lebensohn, and C.N. Tomé: *Mater. Sci. Eng. A: Struct. Mater.: Prop. Microstr. Processing,* 1994, vol. A175, pp. 71-82.
14. I. Karaman, H. Sehitoglu, A.J. Beaudoin, Y.I. Chumlyahov, H.J. Maier, and C.N. Tomé: *Acta Mater.,* 2000, vol. 48 (13), pp. 3311-26.
15. J.D. Eshelby: *Proc. R. Soc.,* London, 1957, vol. A241, p. 398.
16. J.D. Eshelby: *Proc. Progress in Solid Mechanics,* North-Holland, 1961, pp. 89-140.
17. Y. Estrin, and H. Mecking: *Acta Metall.,* 1984, vol. 32 (1), pp. 57-70.
18. H. Mecking, and Y. Estrin: *Proc. Constitutive Relations and Their Physical Basis: Proc. 8th Risø Int. Symp. on Metallurgy and Materials Science,* Risø National Laboratory, Roskilde, Denmark, 1987, pp. 123-45.
19. H. Mecking, and U.F. Kocks: *Acta Metall.,* 1981, vol. 29, pp. 1865-75.
20. A. Acharya and A.J. Beaudoin: *J. Mech. Phys. Solids,* 2000, vol. 48 (10), pp. 2213-30.
21. E. Voce: *J. Inst. Met.,* 1948, vol. 74, pp. 537-62.
22. M.T. Lyttle, and J.A. Wert: *Metall. Mater. Trans. A,* 1999, vol. 30A, pp. 1283-88.
23. H. Fujita, and T. Tabata: *Acta Metall.,* 1973, vol. 21, pp. 355-65.
24. T. Tabata, S. Yamanaka, and H. Fujita: *Acta Metall.,* 1978, vol. 26, pp. 405-11
25. H.K. Hardy: *J. Inst. Met.,* 1951, vol. 79, pp. 321-69.